JOURNAL OF AIRCRAFT
Vol. 46, No. 2, March–April 2009

Three-Dimensional Trajectory Optimization in Constrained Airspace

Ran Dai* and John E. Cochran Jr.†
Auburn University, Auburn, Alabama 36849

DOI: 10.2514/1.39327

The operational airspace of aerospace vehicles, including airplanes and unmanned aerial vehicles, is often restricted so that constraints on three-dimensional climbs, descents, and other maneuvers are necessary. In this paper, the problem of determining constrained, three-dimensional, minimum time-to-climb, and minimum fuel-to-climb trajectories for an aircraft in an airspace defined by a rectangular prism of arbitrary height is considered. The optimal control problem is transformed to a parameter optimization problem. Because a helical geometry appears to be a natural choice for climbing and descending trajectories subject to horizontal constraints, helical curves are chosen as starting trajectories. A procedure for solving the minimum time-to-climb and minimum fuel-to-climb problems by using the direct collocation and nonlinear programming methods including Chebyshev pseudospectral and Gauss pseudospectral discretization is discussed. Results obtained when different constraints are placed on airspace and state variables are presented to show their effect on the performance index. The question of "optimality" of the numerical results is also considered.

I. Introduction

SINCE the 1960's, the minimum time-to-climb (MTTC) and minimum fuel-to-climb (MFTC) problems have attracted the interest of many researchers. Most early investigations were focused on two-dimensional (2-D) MTTC or MFTC formulated as an indirect optimal control problem leading to a two-point boundary value problem (TPBVP) model. To obtain numerical solutions to these problems, Bryson and Denham [1] used the steepest-ascent method, while Calise [2] applied singular perturbation techniques, and Ardema [3] used matched asymptotic expansions to get approximate analytical solutions. Although these and other investigators [4,5] were successful, it is well known that finding the solutions to indirect TPBVPs is very difficult because the solution is very sensitive to changes in the initial values of the adjoint variables. In most cases, when random initial input is used, more iterations are required and/or convergence to a meaningful solution is not achieved. Considering the complexity of the adjoint equations for three-dimensional (3-D) MTTC and MFTC problems, it is not surprising that estimating of the initial values of the adjoint variables is very difficult.

With the advancement of computing power, the use of direct collocation with nonlinear programming (DCNLP) to convert TPBVPs into nonlinear programming problems (NLPPs), a so-called direct optimal control method is feasible and has been applied widely [6–11]. By discretizing the trajectory into multiple segments, characterized by state and control variables as parameters, a TPBVP is transformed into a problem of determining the parameters that satisfy the constraints. In 2-D MTTC problems, this means finding a parameterized load factor or angle of attack as the control, while minimizing the performance index: the final time. Hargraves and Paris [12] applied the collocation method to solve a 2-D MTTC problem. Their results show that in order for an airplane with modest performance capabilities to climb to a desired altitude, the required horizontal projection of its trajectory is similar in magnitude to its final altitude. In some cases, such long horizontal distances are not available. These restrictions may come from local terrain constraints, radar coverage constraints, or collision avoidance constraints. Considering these limitations, aerospace vehicles cannot be assumed to be free to fly anywhere in a given airspace. Instead, a no-fly zone can be defined geometrically. Then, climbs, descents, and other maneuvers that satisfy the constraints must be determined in three dimensions.

When an airplane is constrained to fly in a constrained airspace, it may expend considerably more fuel in achieving the desired terminal conditions. Generally, one would expect that a 3-D MTTC or MFTC trajectory would have a longer magnitude horizontal projection. That is, considerable turning may be required. Intuitively, a helical trajectory is a reasonable initial guess for an optimal path and helical curves have been used in military and transport aircraft landing [13] to keep aircraft within safe areas and prevent collisions with other airplanes. Here, we address the problem of optimal trajectories based on helical first guesses.

In what follows, we present a version of the 3-D MTTC and MFTC problem and our method of solution. Then, we give some results for different boundary conditions and constraints. Conclusions based on the results for the MTTC and MFTC problems are then presented.

II. Aircraft Mathematical Model

The state equations for a three-dimensional point-mass aircraft model [14] that is commonly used for formulating MTTC and MFTC problems in a flat Earth-fixed reference frame are listed in Eq. (1) and illustrated in Fig. 1:

$$\dot{V} = [(T - D)/W - \sin\gamma]g \qquad \dot{\gamma} = (g/V)[n_V - \cos\gamma]$$
$$\dot{\chi} = (g/V)[n_h/\cos\gamma] \qquad \dot{h} = V\sin\gamma$$
$$\dot{x} = V\cos\gamma\cos\chi \qquad \dot{y} = -V\cos\gamma\sin\chi \tag{1}$$

Here, V is the flight speed; γ is the flight-path angle; χ is the heading angle, h is the altitude, x is the down range of the aircraft, and y is the cross range of the aircraft. Also, T is the magnitude of the thrust, which is assumed to be aligned with the velocity and is determined by Mach number and altitude; D is the drag; W is the weight of the aircraft; and M is the flight Mach number. The two control variables are n_V and n_h, the vertical and horizontal load factors, respectively. The resultant load factor is $n = \sqrt{n_V^2 + n_h^2}$, and the bank angle of the aircraft is $\nu = \arctan(n_h/n_V)$. The lift and drag are assumed to be given by

Presented as Paper 1055 at the 45th AIAA Aerospace Sciences Meeting and Exhibit, Reno, NV, 8–11 January 2007; received 24 June 2008; revision received 9 September 2008; accepted for publication 11 September 2008.

*Graduate Research Assistant, Department of Aerospace Engineering.
†Professor and Head, Department of Aerospace Engineering, Fellow AIAA.

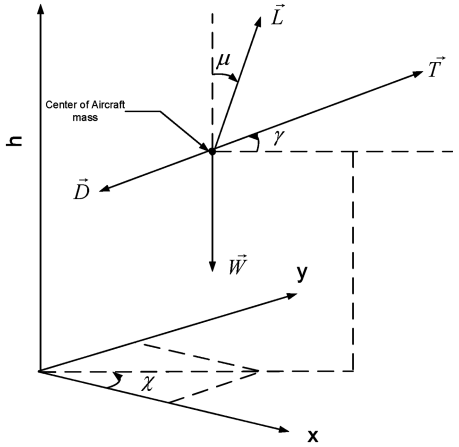

Fig. 1 Three-dimensional aircraft model.

$$L = \frac{1}{2}\rho V^2 S C_{L_\alpha}\alpha \tag{2}$$

and

$$D = \frac{1}{2}\rho V^2 S[C_{D_0} + \eta C_{L_\alpha}\alpha^2] \tag{3}$$

respectively. In Eqs. (2) and (3), ρ is the atmospheric density,S is the reference area for the aerodynamics, C_{L_α} is the lift curve slope, C_{D_0} is the zero lift drag coefficient, η is the drag due to lift factor, and α is the angle of attack (measured from the velocity vector to the zero lift axis). If we let $L = nW$, we may solve Eq. (2) for α and substitute the result into Eq. (3) to obtain

$$D = \frac{1}{2}\rho V^2 S C_{D_0} + \eta\frac{2n^2W^2}{C_{L_\alpha}\rho V^2 S}$$

The numerical results given in this paper were obtained using the data for the thrust magnatude given in Table 1 [4] and the values of C_{L_α}, C_{D_0}, η, weight W, and wing area S given in Table 2 [4]. The 1976 Standard Atmosphere was used as the model for the density ρ.

III. Direct Collocation and Nonlinear Programming

A. Chebyshev Pseudospectral Discretization Method

The basic idea of direct collocation (DC) is to discretize a continuous solution to a problem represented by state and control variables by using linear interpolation to satisfy the differential equations. In this way an optimal control problem (OCP) is transformed into a nonlinear programming problem (NLPP). Because the exact solution to the OCP is in terms of infinitely many values of state and control variables, DC is an approximation.

The well-known discretization methods are trapezoidal, Hermite–Simpson, and Runge–Kutta methods [15], but these methods and some higher-order discretization techniques [9] put the constraints on the defect phase between two adjacent nodes and the distribution of the nodes is arbitrary. That is, it can be dense in one area and sparse in another. On the other hand, we expect that the ideal distribution of the nodes should be fairly uniform within the time interval considered. Thus, the Chebyshev pseudospectral method (CPM) [16–18], which uses Chebyshev–Gauss–Lobatto (CGL) collocation to locate these points, may perform this task better. The standard interval considered here is denoted as $\boldsymbol{\tau} \in [-1, 1]$ with collocation points τ_k set as

$$\tau_k = -\cos(\pi k/N), \qquad k = 0, \ldots, N \tag{5}$$

By using a linear transformation, the actual time $\boldsymbol{t}$ can be expressed as a function of $\boldsymbol{\tau}$ via

$$\boldsymbol{t} = [(t_f - t_0)\boldsymbol{\tau} + (t_f + t_0)]/2 \tag{6}$$

where t_0 is the initial time and t_f is the final time. The state variables $\boldsymbol{x}(\boldsymbol{\tau})$ and control variables $\boldsymbol{u}(\boldsymbol{\tau})$ can then be approximated by Nth-order Lagrange interpolating polynomials

$$\boldsymbol{x}^N(\boldsymbol{\tau}) \approx \sum_{j=0}^{N} \boldsymbol{x}_j \phi_j(\boldsymbol{\tau}) \tag{7}$$

$$\boldsymbol{u}^N(\boldsymbol{\tau}) \approx \sum_{j=0}^{N} \boldsymbol{u}_j \phi_j(\boldsymbol{\tau}) \tag{8}$$

where

$$\phi_j(\boldsymbol{\tau}) = \prod_{\substack{l=1 \\ l\neq j}}^{N} \frac{\boldsymbol{\tau} - \tau_j}{\tau_j - \tau_l} \tag{9}$$

By using Eq. (7), we can express the time derivative of $\boldsymbol{x}^N(\tau_k)$ as the following product of a $(N + 1) \times (N + 1)$ matrix $\boldsymbol{D}$ and $\boldsymbol{x}^N(\tau)$:

Table 1 Thrust as a function of altitude and Mach number from [4] for aircraft 2

Thrust T, thousands of lb												
Mach no. M	Altitude h, thousands of ft											
	0	5	15	25	35	45	55	65	75	85	95	105
0	21.3	20.6	15.4	9.9	5.8	2.9	1.3	0.7	0.3	0.1	0.1	0.0
0.4	22.8	19.8	14.4	9.9	6.2	3.4	1.7	1.0	0.5	0.3	0.1	0.1
0.8	24.5	22.0	16.5	12.0	7.9	4.9	2.8	1.6	0.9	0.5	0.3	0.2
1.2	29.4	27.3	21.0	15.8	11.4	7.2	3.8	2.7	1.6	0.9	0.6	0.4
1.6	29.7	29.0	27.5	21.8	15.7	10.5	6.5	3.8	2.3	1.4	0.8	0.5
2.0	29.9	29.2	28.4	26.6	21.2	14.0	8.7	5.1	3.3	1.9	1.0	0.5
2.4	29.9	29.2	28.4	27.1	25.6	17.2	10.7	6.5	4.1	2.3	1.2	0.5
2.8	29.8	29.1	28.2	26.8	25.6	20.0	12.2	7.6	4.7	2.8	1.4	0.5
3.2	29.7	28.9	27.5	26.1	24.9	20.3	13.0	8.0	4.9	2.8	1.4	0.5

Table 2 Lift and drag coefficients as a function of angle of attack and Mach number for aircraft 2

M	0	0.4	0.8	1.2	1.6	2.0	2.4	2.8	3.2
C_{L_α}	2.240	2.325	2.350	2.290	2.160	1.950	1.700	1.435	1.250
C_{D_0}	0.0065	0.0055	0.0060	0.0118	0.0110	0.0086	0.0074	0.0069	0.0068
			$S = 500$ ft^2		$W = 34,200$ lb	$\eta = 1$			

$$\boldsymbol{s}_k = \frac{\mathrm{d}}{\mathrm{d}t}\boldsymbol{x}^N(\tau_k) = \sum_{j=0}^{N} \boldsymbol{x}_j \frac{\mathrm{d}}{\mathrm{d}t}\phi_j(\tau_k) = \sum_{j=0}^{N} D_{kj}\boldsymbol{x}_j, \qquad k = 0, \ldots, N \tag{10}$$

Appropriately, the matrix $\boldsymbol{D}$ is called the differentiation matrix and has the following explicit form for the Chebyshev spectral differentiation matrix:

$$D_{kj} = \begin{cases} -(c_k/c_j)[(-1)^{j+k}/(\tau_k - \tau_j)], & j \neq k \\ -(2N^2+1)/6, & j = k = 0 \\ (2N^2+1)/6, & j = k = N \\ \tau_k/2(1-\tau_k^2), & \text{otherwise} \end{cases} \tag{11}$$

where $c_0 = c_N = 2$ and $c_1 = \ldots = c_{N-1} = 1$. Unlike the trapezoidal and Hermite–Simpson collocation methods, which are based on forcing the defect vector of midpoints to be zero to satisfy the system differential equations, the CPM enforces constraints directly at the CGL points selected by

$$\boldsymbol{d}_k = \boldsymbol{s}_k - \frac{t_f - t_0}{2}\boldsymbol{f}(\boldsymbol{x}_k, \boldsymbol{u}_k, t_k) = 0 \qquad k = 0, \ldots, N \tag{12}$$

Then, the derivative of the state variables can be calculated using these nodes themselves with the differentiation matrix. In this way, the CPM generally achieves a higher degree of accuracy using orthogonal polynomials instead of the numerical integration polynomials.

B. Gauss Pseudospectral Discretization Method

The Gauss Pseudospectral Method [19,20] (GPM) also uses Lagrange interpolating polynomials to approximate the state and control variables. The GPM differs from the CPM in that its discretization nodes are not exactly the collocation points. In GPM, $N-2$ collocation points are evaluated at the Legendre–Gauss points that lie on the universal time interval $\boldsymbol{\tau} \in [-1, 1]$. The discretization points include the $N-2$ collocation points, the initial point at starting time t_0, and the final point at ending time t_f. Then, the state and control variables are approximated by

$$\boldsymbol{x}(\boldsymbol{\tau}) \approx \sum_{j=0}^{N-2} \boldsymbol{x}_j \phi_j(\boldsymbol{\tau}) \tag{13}$$

$$\boldsymbol{u}(\boldsymbol{\tau}) \approx \sum_{j=1}^{N-2} \boldsymbol{u}_j \phi_j(\boldsymbol{\tau}) \tag{14}$$

and the system equality constraints at these collocation points are expressed as

$$\boldsymbol{d}_k = \sum_{i=0}^{N-2} D_{ki}\boldsymbol{x}_i - \frac{t_f - t_0}{2}\boldsymbol{f}(\boldsymbol{x}_k, \boldsymbol{u}_k, t_k) = 0 \qquad k = 1, \ldots, N-2 \tag{15}$$

There are additional constraints that must be enforced at the final time state variable $\boldsymbol{x}_f$ by the Gauss quadrature integration of the dynamics over the entire time interval

$$\boldsymbol{d}_{N-1} = \boldsymbol{x}_f - \boldsymbol{x}_0 - \frac{t_f - t_0}{2}\sum_{k=1}^{N-2} w_k \boldsymbol{f}(\boldsymbol{x}_k, \boldsymbol{u}_k, t_k) = 0 \tag{16}$$

Here, w_k is the Gauss weights and is defined as

$$w_k = \frac{2}{1-\tau_k^2}[\dot{P}_N(\tau_k)]^2 \tag{17}$$

where $\dot{P}_N$ is the derivative of the Legendre polynomial of degree N. As illustrated in [20,21], the costate mapping when GPM is used has higher accuracy than when other pseudospectral methods are applied. Hence, it was introduced previously to evaluate the costates and show, later, that certain optimality conditions are satisfied.

C. Nonlinear Programming Solver: SNOPT 6.2

The nonlinear programming (NLP) solver used to solve the NLPP considered in this work is based on a sequential quadrature programming (SQP) algorithm and is called SNOPT [22,23]. SNOPT can be used to solve problems such as to minimize a performance index $J(\boldsymbol{x})$, subject to constraints on individual state and/or control variables

$$\boldsymbol{x}_L \leq \boldsymbol{x} \leq \boldsymbol{x}_U \tag{18}$$

constraints defined by linear combinations of state and/or control variables:

$$\boldsymbol{b}_L \leq \boldsymbol{A}\boldsymbol{x} \leq \boldsymbol{b}_U \tag{19}$$

and/or constraints defined by nonlinear functions of state and/or control variables:

$$\boldsymbol{c}_L \leq \boldsymbol{c}(\boldsymbol{x}) \leq \boldsymbol{c}_U \tag{20}$$

The 3-D MTTC problem may be transformed into this standard form. The problem is to minimize $J = t_f - t_0$ with all NLP variables

$$\boldsymbol{x} = \begin{cases} \lfloor \boldsymbol{x}_0, \boldsymbol{x}_1, \boldsymbol{x}_2, \cdots \boldsymbol{x}_k, \boldsymbol{x}_{k+1}, \cdots \boldsymbol{x}_{N-1}, \boldsymbol{x}_N, \boldsymbol{u}_0, \boldsymbol{u}_1, \boldsymbol{u}_2, \cdots \boldsymbol{u}_k, \boldsymbol{u}_{k+1}, \cdots, \boldsymbol{u}_{N-1}, \boldsymbol{u}_N, t_0, t_f \rfloor & \text{in CPM} \\ [\boldsymbol{x}_0, \boldsymbol{x}_1, \boldsymbol{x}_2, \cdots \boldsymbol{x}_k, \boldsymbol{x}_{k+1}, \cdots, \boldsymbol{x}_{N-3}, \boldsymbol{x}_{N-2}, \boldsymbol{x}_f, \boldsymbol{u}_1, \boldsymbol{u}_2, \cdots \boldsymbol{u}_k, \boldsymbol{u}_{k+1}, \cdots, \boldsymbol{u}_{N-3}, \boldsymbol{u}_{N-2}, t_0, t_f] & \text{in GPM} \end{cases} \tag{21}$$

where lower bound $\leq \boldsymbol{x} \leq$ upper bound, subject to the nonlinear constraints:

$$\boldsymbol{d}_k = \boldsymbol{c}_U = \boldsymbol{c}_L = 0 \tag{22}$$

where $k = 0, \ldots, N$ in CPM and $k = 1, \ldots, N-1$ in GPM. In this way, the dynamic system equations will be defined as nonlinear constraints together with state variable constraints.

IV. Two-Dimensional Minimum Time-to-Climb Problem

To illustrate the differences in 2-D and 3-D trajectories, it is best to start with the 2-D MTTC problem. Here, the state variables are reduced to four: V, γ, h, and x. One control variable is n, the load factor, the reformulated equations are

$$\begin{gathered} \dot{V} = [(T(M,h) - D(M,h,n))/W - \sin\gamma]g \\ \dot{\gamma} = (g/V)[n - \cos\gamma] \qquad \dot{h} = V\sin\gamma \qquad \dot{x} = V\cos\gamma \end{gathered} \tag{23}$$

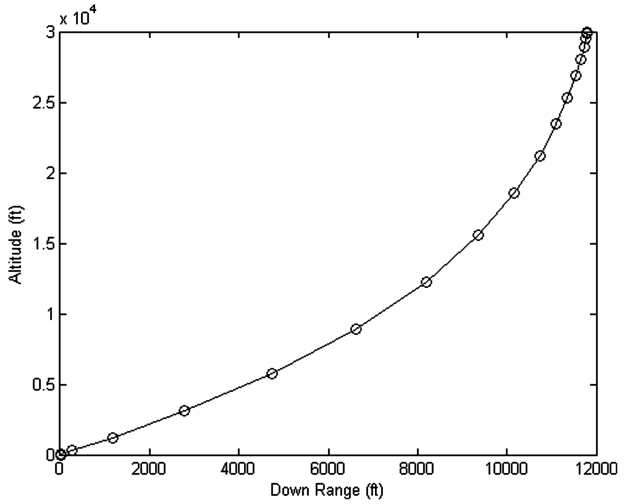

Fig. 2 2-D MTTC altitude and down-range trajectory using DCNLP method.

The other properties are the same as for the 3-D problem. An example of optimal trajectory was calculated using the DCNLP method with initial and final conditions defined as

$$V(0) = 558.2 \text{ ft/s} \qquad h(0) = 0$$
$$\gamma(0) = 0 \qquad h_{t_f} = 30,000 \text{ ft} \tag{24}$$

The minimum time obtained is 72.81 s with boundary constraints and system equality constraints well satisfied. The MTTC trajectory of an altitude–down range plot is shown in Fig. 2. It can be seen from the footprint that in order for an aircraft with modest performance most of the time to climb from sea level to the desired altitude of 30,000 ft, its horizontal displacement will be almost half of the altitude gained even with a fast initial speed. That is because most of the time the aircraft's flight-path angle is less than $\pi/3$, making the projection of the trajectory as long as almost half of the magnitude of the altitude change. If the initial speed is lower, the down range projection will be even longer. In some cases, such long horizontal distance is not available. In those cases it is necessary for the aircraft to make some turns to avoid violating the airspace restrictions. Hence, the preceding 3-D aircraft model is used to determine the maneuvers and types of trajectories needed for climbs within constrained airspace.

V. Initial Nonlinear Programming Variable Inputs

Although in most cases the choice of initial input of the NLP variables is arbitrary, a good guess will improve the rate of convergence and the probability of getting a good result. Assuming that the aircraft is climbing inside a cylinder with square projection in the x-y plane, to allow for a large enough horizontal flight distance, the final trajectory will make good use of the constrained airspace as much as possible. From the 2-D optimal trajectory, the horizontal projection is almost half of its final altitude. Because of the space constraints, the 3-D trajectory horizontal projection is expected to be greater than that of a 2-D trajectory that had the same final altitude. That is because part of the lift force in the 2-D trajectory is spent on generating the turning force to avoid collision with the bounds, which makes the aircraft travel a longer horizontal distance to achieve the same altitude. The 3-D horizontal projection on the x-y plane is a circular curve with the same radius as one-half of a side of the base if the aircraft is expected to travel as far as possible in designed turning angle. Expanding the horizontal projection in a vertical direction turns to be a helical curve wrapped on a right-circular cylinder with radius R enclosed within the square cylinder, as shown in Fig. 3. As a starting point, we assume that the helix curve is transversed with constant velocity and inclination angle. Then, the system equations of motion can be simplified to get

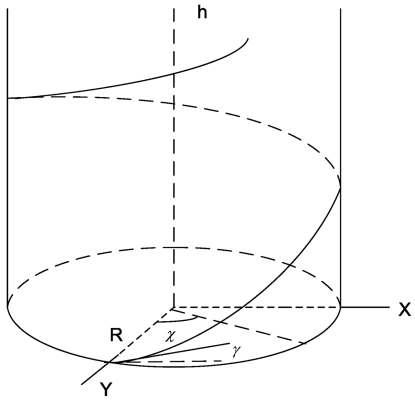

Fig. 3 Circular helix curve wrapped on a cylinder.

$$\dot{V} = 0 \Rightarrow V = V_I \qquad \dot{\gamma} = 0 \Rightarrow \gamma = \gamma_I \qquad \dot{\chi} = V_I \cos\gamma / R$$
$$\dot{h} = V \sin\gamma \Rightarrow h = V_I t \sin\gamma \qquad x = R \sin\gamma \qquad y = R \cos\gamma \tag{25}$$

where V_I and γ_I are the preassumed constant velocity and constant flight-path angle of the aircraft. Normally, they are assumed to be the takeoff velocity and flight-path angle, separately. If the time intervals are chosen as Chebyshev or Gauss points, then all the initial NLP variables can be fixed according to Eq. (25). In all of the following cases, the first initial guess uses 22 discretization nodes selected according to this simplified model. After that the number of nodes is doubled and these nodes are interpolated using the results obtained in the first calculation. Finally, the trajectory is refined with a high number of nodes and relatively fast convergence.

VI. Results for 3-D MTTC and MFTC Problems

A. 3-D MTTC Problem

In this section, we present some results for 3-D MTTC problems in the form of a collection of trajectories in different types of constrained airspaces. The boundary constraints and performance limitations are those listed in Table 3.

Case 1: Set the airspace constraints on x and y as $\pm 10,000$ ft. The aircraft is required to fly from sea level to an altitude of $h_f = 30,000$ ft with an initial flight speed of Mach $= 0.5$, an initial flight-path angle of $\gamma_0 = 12.6$ deg, and an initial heading angle of $\chi_0 = 0$. The minimum time obtained for this case is 89.76 s using CPM and 89.87 s using GPM. The three-dimensional trajectory is shown in Fig. 4, and the time histories of vertical and horizontal load factors n_V and n_h, velocity V, flight-path angle γ, and heading angle χ are shown in Fig. 5 for CPM. The corresponding results for GPM are shown in Figs. 6 and 7. From the plots, it is obvious that the two discretization methods produce very similar results. For conciseness, in the additional cases, only the CPM plots are presented and both the CPM and GPM results are summarized and compared in Table 4. The performance index minimum time increased 16.95 s, which is 23.28% of the time required in 2-D MTTC results. So the constraints

Table 3 Boundary conditions and performance limitations for 3-D MTTC problem

Constraints	Values
Initial coordinate constraints	$x = x_0, y = y_0, h = 0$
Initial V ,γ, and χ constraints	$V = V_0, \gamma = \gamma_0, \chi = \chi_0$
Final altitude	$h = h_f$
Airspace constraints	$x_{\min} \le x \le x_{\max}, y_{\min} \le y \le y_{\max}$
Maximum and minimum vertical load factor	$n_{v\max} = 10, n_{v\min} = -10$
Maximum and minimum horizontal load factor	$n_{h\max} = 10, n_{h\min} = -10$

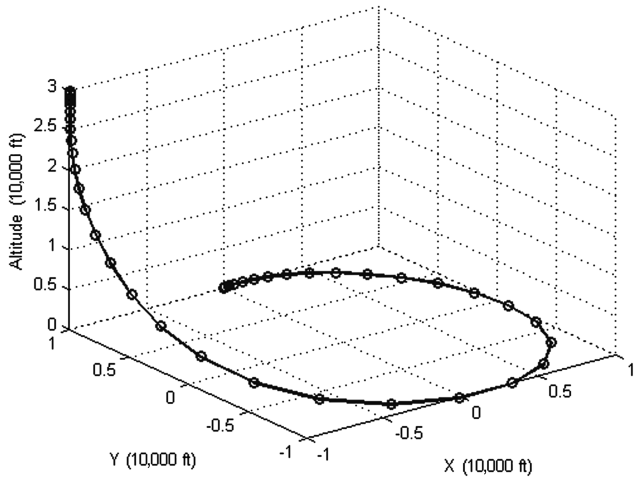

Fig. 4 3-D MTTC trajectory for case 1 using CPM.

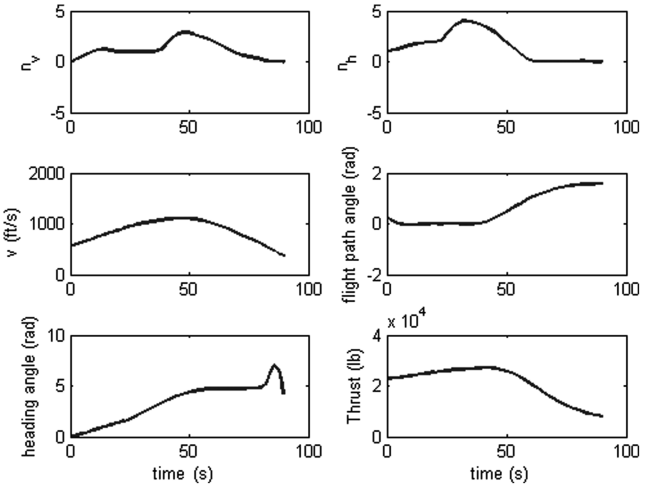

Fig. 5 Control and state variables history for case 1 using CPM.

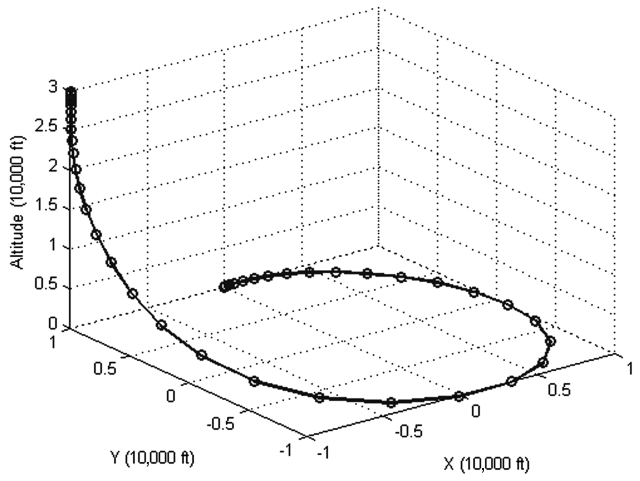

Fig. 6 3-D MTTC trajectory for case 1 using GPM.

on the airspace volume caused obvious an difference on the performance index.

Case 2: When the final 30,000 ft altitude was reached under the same initial condition of case 1 and with the constraints on both x and y of $\pm 7,500$ ft, the minimum time calculated here is 125.24 s. The trajectory and corresponding state and control variable time histories are shown in Figs. 8 and 9, respectively. It can be seen when the wide

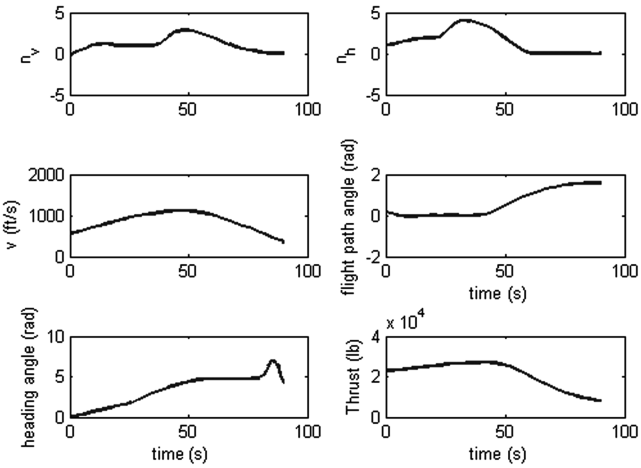

Fig. 7 Control and state variables history for case 1 using GPM.

square base is not available, instead the width is constrained to 75% of the original one, the minimum time increases by 39.53%.

Case 3: When the final flight speed constraint of Mach = 0.8 is added to case 2, the optimal climb time changes to 175.28 s. The trajectory and corresponding state and control variable time histories are shown in Figs. 10 and 11, respectively. The speed profile in Fig. 9 of case 2 approaches zero at the ending point, the constraint on the final speed avoids this stall point but results in the sacrifice of spending 39.96% more time in the climb than in case 2.

B. 3-D MFTC Problem

In the 3-D MTTC problem, the aircraft's weight is treated as a constant. Actually, the consumption of the fuel during this time interval makes the weight of the aircraft a function of time. The change of the weight is omitted in preceding discussion because the climb task is completed in a couple of minutes, which makes this change of weight small. However, multiple climbs may be necessary in a given mission and fuel consumption may be the principal concern. Here, the variation of weight is included in the model by assuming that

$$\dot{m} = -f = -T/cg \tag{26}$$

where $c = 2,800$ s and f is the fuel consumption rate, and the mass is added as an additional state variable to the pervious 6×1 state variable vector. The other system equations are symbolically the same with the weight considered as a function of time $W(t)$ with the initial value, $W_0 = 34,200$ lb. The objective function is the final weight

$$J = -W_f \tag{27}$$

Results for some cases are tested with the same boundary constraints and performance limitations used in previous MTTC problems were obtained for comparison.

Case 4: The same initial and final conditions and airspace constraints as in case 1 with unspecified climb time were used. Transversal of the MFTC trajectory required similar time, 93.13 s, when compared with case 1 with the final weight of 33,546.5 lb and fuel consumption of 653.5 lb. If other aircrafts are involved in this constrained space at the same time, the volume specified here is not available all the time due to other traffic occupying part of this space. To prevent collisions with other traffic, the aircraft taking off at latter time has to make horizontal circles or climb with a constrained flight-path angle to allow for the earlier taking-off aircrafts climbing first. To estimate the effect of this constraint on the fuel consumption, a maximum flight-path angle of 36 deg is added to case 4 and the trajectory, corresponding state and control variable time histories are shown in Figs. 12 and 13 together with the results of the free flight-path angle, respectively. The final weight of the aircraft with flight-path angle constraints is 33,439.6 lb and the fuel consumption

Table 4 CPM and GPM optimal results comparison

Performance	Case 1	Case 2	Case 3	Case 4	Case 5
CPM	$t_{\min} = 89.76$ s	$t_{\min} = 125.24$ s	$t_{\min} = 175.28$ s	$W_{\max} = 33,546.5$ lb	$W_{\max} = 33,507.5$ lb
GPM	$t_{\min} = 89.87$ s	$t_{\min} = 125.78$ s	$t_{\min} = 175.38$ s	$W_{\max} = 33,546.5$ lb	$W_{\max} = 33,498.3$ lb

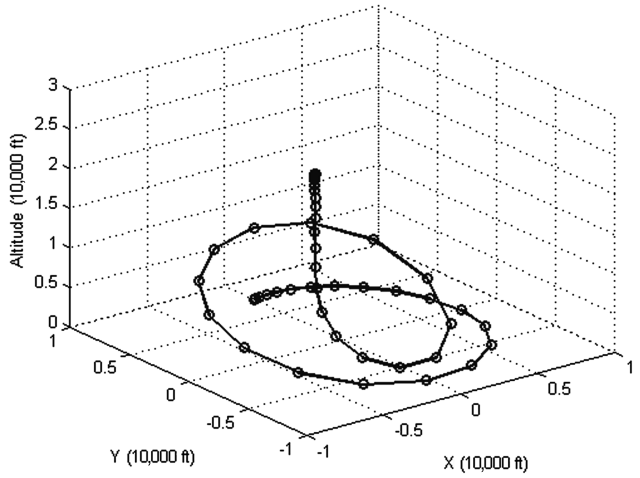

Fig. 8 3-D MTTC trajectory for case 2 using CPM.

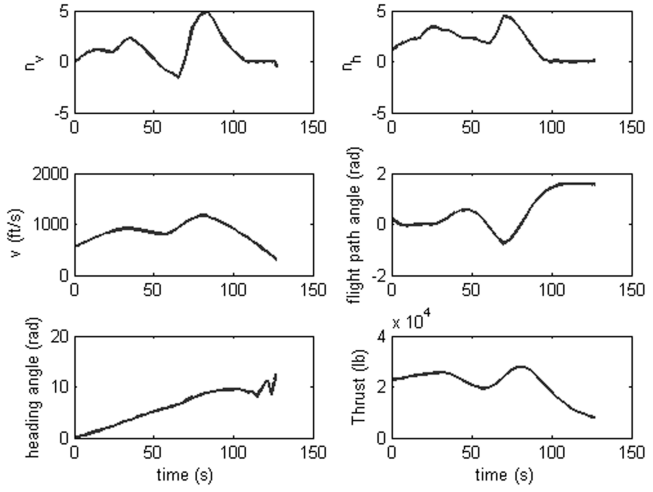

Fig. 9 Control and state variables history for case 2 using CPM.

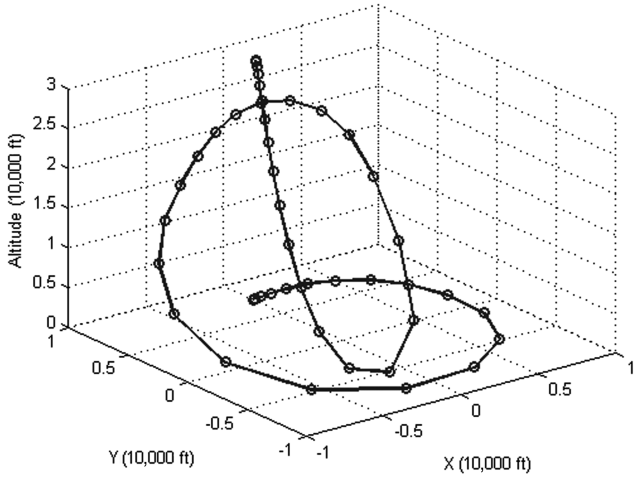

Fig. 10 3-D MTTC trajectory for case 3 using CPM.

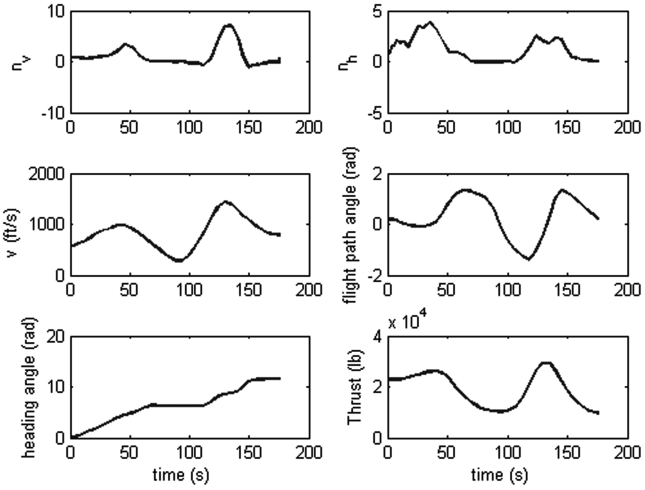

Fig. 11 Control and state variables history for case 3 using CPM.

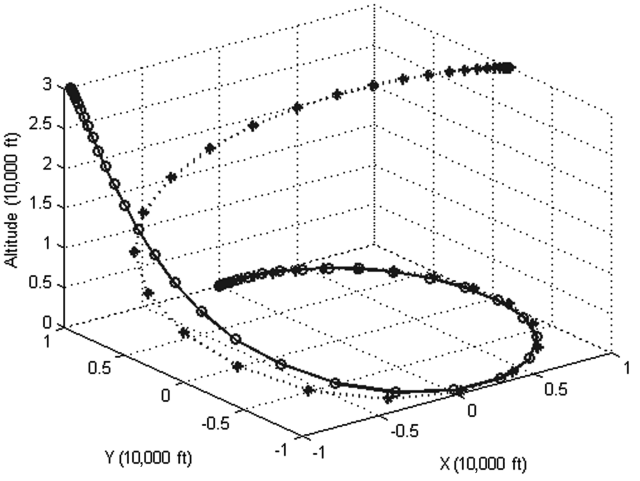

Fig. 12 3-D MFTC trajectory for case 4 with (dotted line) and without (solid line) flight-path angle constraint using CPM.

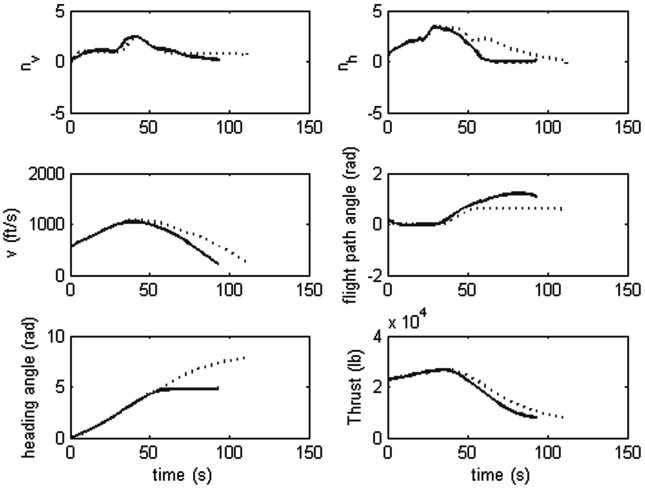

Fig. 13 Control and state variables history for case 4 with (dotted line) and without (solid line) flight-path angle constraint using CPM.

is 760.4 lb, which is 16.36% more than the single aircraft consumption.

Case 5: The preceding MFTC case considers only an unspecified final time; the NLP solver will choose the optimized time to get the minimum fuel results. When the final time is specified as 100 s in case 4, the consumption of fuel is more than previous results, and the final weight is reduced to 33,507.5 lb and the fuel consumption increased to 507.5 lb. The trajectory with flight-path angle constraints and the designated flight time of 120 s will end with 33,418.0 lb and a fuel consumption of 781.99 lb, which is 54.09% more than the consumption without flight-path angle constraints. The MFTC trajectories, corresponding state and control variable time histories with and without flight-path angle constraints are shown in Figs. 14 and 15, respectively.

C. Optimality

To show that the results obtained from the DCNLP method are optimal within the precision of the numerical calculations, we consider the Hamiltonian formulation of the optimal control problem. If the solutions are optimal, then the DCNLP discrete state and control variables should be good approximations to the solutions to the indirect optimal control problem at the collocation points. There are ways [21,24] to estimate the costates and Lagrange multipliers related to the path constraints at the collocation points according to different discretization methods. In the two methods used previously, only the GPM has been used to address the problem of estimating the costate. However, because the results obtained for the states and controls using the CPM and the GPM methods are very close, proving those from one are optimal should be sufficient. In the following, the GPM trajectory optimality proof will be provided.

The Hamiltonian for the 3-D MTTC problem may be written as

$$H_k = 1 + \lambda_{Vk}\left(\frac{T_k - D_k}{W} - \sin\gamma_k\right)g + \lambda_{\gamma k}(g/V_k)[n_{Vk} - \cos\gamma_k] + \lambda_{\chi k}(g/V_k)[n_{hk}/\cos\gamma_k] + \lambda_{xk}V_k\cos\gamma_k\cos\chi_k + \lambda_{hk}V_k\sin\gamma_k - \lambda_{yk}V_k\cos\gamma_k\sin\chi_k + \boldsymbol{\upsilon}_k\boldsymbol{C}_k,$$
$$k = 1,\ldots,N-2 \tag{28}$$

The costate vector is $\boldsymbol{\lambda}_k = [\lambda_{Vk}, \lambda_{\gamma k}, \lambda_{\chi k}, \lambda_{hk}, \lambda_{xk}, \lambda_{yk}]^T$ and $\boldsymbol{\upsilon}_k$ is the Lagrange multiplier vector associated with the path constraints vector $\boldsymbol{C}_k$ at collocation point k. When an optimal solution is obtained by the NLP solver, it will provide costates $\tilde{\boldsymbol{\lambda}}_k$ together with Lagrange multipliers $\tilde{\boldsymbol{\upsilon}}_k$ at each collocation point, which are called Karush–Kuhn–Tucker (KKT) multipliers. These KKT multipliers satisfy the necessary optimal conditions of the NLP problem formulated previously. Then, the costates and the Lagrange multipliers at collocation points can be estimated by using the KKT multipliers in the following simple transformation [21]:

$$\boldsymbol{\lambda}_k = \frac{\tilde{\boldsymbol{\lambda}}_k}{w_k} + \tilde{\boldsymbol{\lambda}}_f \qquad \boldsymbol{\lambda}(t_0) = \tilde{\boldsymbol{\lambda}}_0, \qquad \boldsymbol{\upsilon}_k = \frac{2}{t_f - t_0}\frac{\tilde{\boldsymbol{\upsilon}}_k}{w_k} \qquad \boldsymbol{\lambda}(t_f) = \tilde{\boldsymbol{\lambda}}_f \tag{29}$$

Pontryagin's minimum principle [22] requires the control variables to minimize the Hamiltonian along the optimal trajectory at every point in time. Also, the Hamiltonian final value conditions indicate that for a minimum time problem $H(t_f) = 0$. From Eq. (29), it can be seen that the Hamiltonian is not explicitly a function of time, and so it is constant. Hence, the Hamiltonian should be identically zero. For the case 1 3-D MTTC problem, the costates and the Hamiltonian were calculated and are shown in Fig. 16. In this case, the Hamiltonian is very close to zero at all discretization points. This result along with the approximate equality of the states is sufficient evidence of the optimality of the DCNLP solution. The other cases can be verified in the same way.

D. Discussion of Results

The final trajectories are similar to a helical curve wrapped on a cylinder, which makes the guess of the helical trajectory as an initial input reasonable. The CPM and GPM methods showed very close results. Cases 1 and 2 reached the same final altitude but had different constrained airspace, and it was shown that smaller constraints will cost more time for an aircraft to climb to a desired altitude.

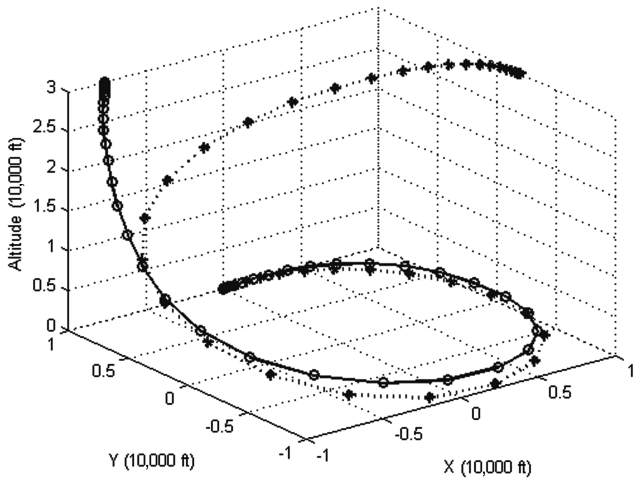

Fig. 14 3-D MFTC trajectory for case 5 with (dotted line) and without (solid line) flight-path angle constraint using CPM.

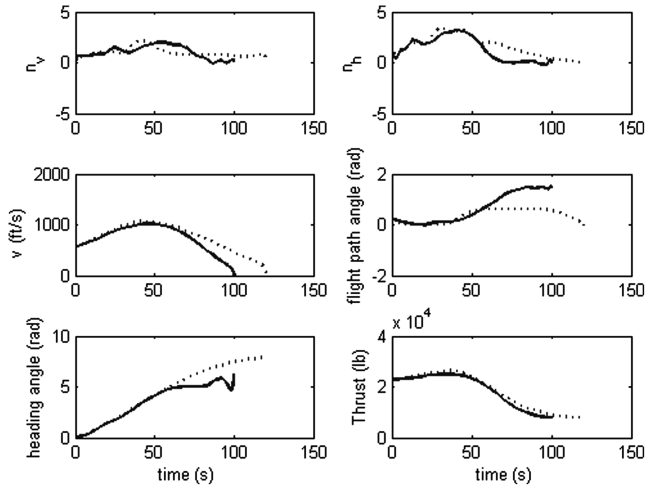

Fig. 15 Control and state variables history for case 5 with (dotted line) and without (solid line) flight-path angle constraint using CPM.

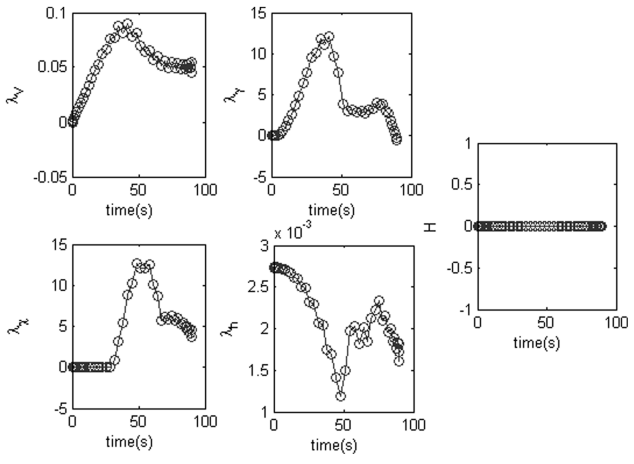

Fig. 16 Costates and Hamiltonian for case 1 using CPM.

The optimized trajectory can be treated as a process of climb–dive–climb. The aircraft stays at sea level initially to gain speed and then makes a fast climb. In some cases the aircraft's speed will reduce to close to zero before it reaches the final altitude. To complete the climb task, it is necessary to make a dive to gain speed and then climb again. Cases 2 and 3 illustrate this relation. When higher altitudes are required, more dives and climbs may be performed. That is why the trajectory is a repeat process of climb–dive–climb.

In the MFTC problem, the trajectory of case 4 is similar to the trajectory of case 1, and the mass of the aircraft changes in a small scale, which can be negligible. To obtain the objective of minimum fuel consumption in the climb procedure, it is expected that the aircraft can reach the final altitude in the least time to consume as little as possible fuel. From this point of view, it is reasonable that the MTTC trajectory and MFTC trajectory are close to each other if the task is completed in a short period of time. The results for case 5 show that any specified time larger than that for the unspecified final time result will cost more fuel consumption.

From all of the presented trajectories and corresponding performance index data, it can be seen that a smaller volume of the airspace constraints or additional bounds of the state variables will make the previous trajectory deviate from the original optimized solution and cost more time or fuel to achieve the same altitude. The time increase percentage between Cases 1 and 2, Cases 2 and 3 shows the effect of airspace constraints and final speed constraints on the climbing time. The fuel consumption increase percentage of case 4 and case 5 with and without flight-path angle constraints shows the effect of the availability of the specified airspace on the fuel consumption. All of these data illustrates that a small difference of the specified constraints will cost a relatively high percentage of the performance index to achieve the same objective while satisfying the new constraints.

VII. Conclusions

The contribution of this paper includes two sides. Theoretically, it expands from a two-dimensional to a three-dimension aircraft model and starts from a helical curve as an initial guess, then uses the Chebyshev pseudospectral method, Gauss pseudospectral method, and nonlinear programming solver to solve the three-dimensional minimum time-to-climb and minimum fuel-to-climb problems under different assumption conditions. The optimality of the trajectories was considered, and numerical evidence of the optimality was obtained by estimating the costate variables and the Hamiltonian. The results show that the performance index, the climb time, may be found while system equality constraints, boundary constraints, and control constraints are satisfied. Practically, this paper considers different constraints' effects on the performance index and illustrates their importance on maintaining a high performance maneuver, which will improve the efficiency in aircraft task performance. Future research will focus on a moving target in a small area under the same constraints, which means a feedback of the sensed target state is required to form a closed-loop system to catch this moving target.

References

[1] Bryson, A. E., and Denham, W. F., "A Steepest-Ascent Method for Solving Optimum Programming Programs," *Journal of Applied Mechanics*, Vol. 29, No. 2, June 1962, pp. 247–257.

[2] Calise, A. J., "Extended Energy Management for Flight Performance Optimization," *AIAA Journal*, Vol. 15, No. 3, March 1977, pp. 314–321. doi:10.2514/3.63239

[3] Ardema, M. D., "Solution of the Minimum-Time-to-Climb Problem by Matched Asymptotic Expansions," *AIAA Journal*, Vol. 14, No. 7, 1976, pp. 843–850. doi:10.2514/3.7161

[4] Bryson, A. E., Desai, M. N., and Hoffman, W. C., "Energy-State Approximation in Performance Optimization of Supersonic Aircraft," *Journal of Aircraft*, Vol. 6, No. 6, 1969, pp. 481–488. doi:10.2514/3.44093

[5] Rao, A. V., and Mease, K. D., "Minimum Time-to-Climb Trajectories Using a Modified Sweep Method," AIAA Paper 95-3263-CP, 1995.

[6] Ringertz, U., "Optimal Trajectory for a Minimum Fuel Turn," *Journal of Aircraft*, Vol. 37, No. 5, 2000, pp. 932–934. doi:10.2514/2.2697

[7] Norsell, M., "Multistage Trajectory Optimization with Radar-Range Constraints," *Journal of Aircraft*, Vol. 42, No. 4, 2005, pp. 849–857. doi:10.2514/1.8544

[8] Williams, P., Sgarioto, D., and Trivailo, P. M., "Constrained Path-Planning for an Aerial-Towed Cable System," *Aerospace Science and Technology*, Vol. 12, No. 5, 2008, pp. 347–354. doi:10.1016/j.ast.2007.08.006

[9] Herman, A. L., and Spencer, D. B., "Optimal, Low-Thrust Earth-Orbit Transfers Using Higher-Order Collocation Methods," *Journal of Guidance, Control, and Dynamics*, Vol. 25, No. 1, 2002, pp. 40–47. doi:10.2514/2.4873

[10] Horie, K., and Conway, B. A., "Optimal, Aeroassisted Orbital Interception," *Journal of Guidance, Control, and Dynamics*, Vol. 22, No. 5, 1999, pp. 625–631. doi:10.2514/2.4435

[11] Geiger, B. R., Horn, J. F., DeLullo, A. M., and Long, L. N., "Optimal Path Planning of UAVs Using Direct Collocation with Nonlinear Programming," *AIAA Guidance, Navigation, and Control Conference and Exhibit*, AIAA Paper 2006-6199, 2006.

[12] Hargraves, C. R., and Paris, S. W., "Direct Trajectory Optimization Using Nonlinear Programming and Collocation," *Journal of Guidance, Control, and Dynamics*, Vol. 10, No. 4, 1987, pp. 338–342. doi:10.2514/3.20223

[13] Crawford, D. J., and Bwoles, R. L., "Automatic Guidance and Control of a Transport Aircraft During a Helical Landing Approach," NASA Technical Report TN D-7098, 1975.

[14] Kumar, R. K., Seywald, H., and Cliff, E. M., "Near-Optimal Three-Dimensional Air-to-Air Missile Guidance Against Maneuvering Target," *Journal of Guidance, Control, and Dynamics*, Vol. 18, No. 3, 1995, pp. 457–464. doi:10.2514/3.21409

[15] Betts, J. T., and Huffman, W. P., "Path-Constrained Trajectory Optimization Using Sparse Sequential Quadratic Programming," *Journal of Guidance, Control, and Dynamics*, Vol. 16, No. 1, 1993, pp. 59–68. doi:10.2514/3.11428

[16] Fahroo, M., and Ross, I. M., "Direct Trajectory Optimization by a Chebychev Pseudospectral Method," *Journal of Guidance, Control, and Dynamics*, Vol. 25, No. 1, 2002, pp. 160–166. doi:10.2514/2.4862

[17] Trefethen, L. N., *Spectral Methods in MATLAB*, Society for Industrial and Applied Mathematics, Philadelphia, 2000.

[18] Pietz, J. A., "Pseudospectral Collocation Methods for the Direct Transcription of Optimal Control Problems," M.A. Thesis, Department of Computational and Applied Mathematics, Rice University, Houston, TX, 2003.

[19] Ben, D.,"A Gauss Pseudospectral Transcription for Optimal Control," Ph.D. Dissertation, Department of Aeronautics and Astronautics, Massachusetts Institute of Technology, Nov. 2004.

[20] Benson, D. A., Huntington, G. T., Thorvaldsen, T. P., and Rao, A. V., "Direct Trajectory Optimization and Costate Estimation via an Orthogonal Collocation Method," *Journal of Guidance, Control, and Dynamics*, Vol. 27, No. 3, 2004, pp. 397–405. doi:10.2514/1.3426

[21] Huntington, G. T., Benson, D. A., and Rao, A. V., "A Comparison of Accuracy and Computational Efficiency of Three Pseudospectral Methods," AIAA Paper 2007-6405, Aug. 2007.

[22] Gano, S. E., Perez, V. M., and Renaud, J. E., "Development and Verification of a MATLAB Driver for the SNOPT Optimization Software," AIAA Paper 2001-1620, 2001.

[23] Holmstrom, K., Goran, A. O., and Edvall, M. M., "User's Guide For TOMLAB /SNOPT," Tomlab Optimization, Inc., 2005, http://tomlab.biz [retrieved 1 May 2008].

[24] Fahroo, F., and Ross, I. M., "Costate Estimation by a Legendre Pseudospectral Method," *Journal of Guidance, Control, and Dynamics*, Vol. 24, No. 2, 2001, pp. 270–277. doi:10.2514/2.4709